Оптический журнал

Иконика

УДК 535; 535.3; 543.4

Быстрое восстановление изображения с использованием метода фазового разнесения для простой оптической системы

© 2022 г. Wenbo Jing, Genming Cao, Bingkun Huang, Jiaming Zhang, Shiyao Tian, and Caixia Wang

Предложен метод восстановления изображения для исправления фиксированной оптической аберрации простой оптической системы с использованием двухканального фазового разнесения и калиброванного коэффициента одноканального восстановления для ускорения восстановления изображения. Функция рассеяния точки, которая оценивается заранее с помощью двухканального фазового разнесения, служит известным ядром размытия простой оптической системы. Выполнен расчет коэффициента одноканального восстановления в частотной области простой оптической системы для быстрого восстановление нерезкого изображения. Предлагаемый подход, требующий только двойного преобразования Фурье без итеративной оптимизации, выполняет прямое и быстрое восстановление нерезкого изображения. Выполненные эксперименты показывают, что предложенный метод действительно может обеспечить качество изображения, сравнимое с двухканальным восстановлением изображения, при значительном сокращении времени обработки.

Ключевые слова: *простая оптическая система, восстановление изображения, фазовое разнесение, оптическая аберрация*

Fast image restoration method for a simple optical system using phase diversity technique

© 2022 W. B. Jing*, PhD (Engineering); G. M. Cao*, postgraduate student (Engineering); B. K. Huang*, postgraduate student (Engineering); J. M. Zhang**, postgraduate student (Engineering); S. Y. Tian*, postgraduate student (Engineering); C. X. Wang**, PhD (Engineering)

*School of Opto-Electronic Engineering, Changchun University of Science and Technology, Changchun, Jilin, China

**School of Electronic Information and Engineering, Changchun University of Science and Technology, Changchun, Jilin, China

E-mail: wenbojing@cust.edu.cn

Submitted 12.08.2021

DOI:10.17586/1023-5086-2022-89-01-33-46

We propose an image restoration method for correcting the fixed optical aberration of the simple optical system using the dual-channel phase diversity and the calibrated single-channel restoration factor to speed up the image restoration. The point-spread function, which is estimated in advance with the dual-channel phase diversity, serves as the known blur kernel of the simple

optical system. In the frequency domain, the single-channel restoration factor of the simple optical system is constructed to restore the blurred image quickly. Our approach needing only twice Fourier transforms without iterative optimization can directly and rapidly restore the blurred image of the simple optical system. The experimental results are performed to verify the fast image restoration ability of the single-channel fast image restoration. The experimental results indicate that the single-channel fast image restoration can indeed obtain comparable image quality as the dual-channel image restoration, but significantly reduce the time of image restoration.

Keywords: *simple optical system, image restoration, phase diversity, optical aberration.*

OCIS codes: *080.1010, 100.3020, 110.6770, 110.1758*

1. INTRODUCTION

Traditional methods of optical design come at a sacrifice of optical system simplicity for image quality. Computational imaging, which can overcome the limits of physical optics, has emerged with the goal of relaxing the constraints on the imaging hardware, so as to improve the imaging resolution [1, 2], increase the field of view [3] (FOV) or enhance the noise robustness [4, 5].

The telephoto optical system used in unmanned aerial vehicle (UAV) and astronomical exploration has the characteristics of long focal length and small FOV. Thus, it is inevitable that the telephoto optical system is larger, heavier, more complex and expensive than the conventional lens (such as cellphone lens). The simple optical system comprises of few lenses, inevitably expanding the impact of aberration (such as coma, geometric distortion, spherical aberration, and chromatic aberration) with structural simplification. In recent years, high-quality computational imaging is possible through a simple optical system with a lighter weight and less expensive [6–8]. Schuler *et al.* first put forward the idea of a simple optical system with computationally corrected aberrations. Their work presented a method to ease image degradation caused by imperfect optics, which could correct the optical aberrations [6]. Later, a new cross-channel prior to color images on the basis of Schuler's research was proposed, so as to improve simple lens imaging. This prior could handle complex and large blur kernel (or point-spread function, PSF) [7]. Recently, basing on sparse signal representation, a set of computational photography techniques was proposed to remove optical aberrations, which allowed the recovery of images captured through a single-lens camera. Owing to such advantage that many prior PSFs estimated at different depths are successfully used for restoring visual images in a short time, the method can be widely applied in the non-blind deconvolution methods [9]. Because diffractive optical elements can drastically reduce the weight and size of imaging devices compared to their refractive counterparts, they have recently attracted great attention in computational imaging. However, the quality of images acquired by a diffractive optics-based system is strongly influenced by strong distortions. To overcome these problems, various methods have been proposed. For example, Peng *et al.* used diffractive-refractive optics to design lenses with thin structures, and then employed a fast, but robust deconvolution to correct chromatic aberrations introduced by the diffractive phase modulation [10]. Heide *et al.* proposed a method which combined the encoded diffractive designs with a novel computational approach for self-calibrating imaging, so as to restore high-quality images without pre-calibration of the simple optical system [11]. In addition, many deep learning methods have been also used in the image restoration of the simple optical system with the development of deep learning technology [12, 13]. In general, all of these methods for removing a fixed optical aberration of the simple optical system are made up of two major steps. The first step is to estimate the PSF of the simple optical system with a blind deconvolution approach, and the second step is to restore the blurred image with a non-blind deconvolution method. They all can effectively restore the blurred image of the simple optical system. However, these methods are complicated, time-consuming, and therefore unsuitable for real-time imaging. It is worth noting that Schmidt *et al.* put forward the method of real-time image restoration methods using multi-frame images for online blind convolution

and contrast enhancement [14]. But the reasonable guess of the PSF is important for the recovery speed of image restoration.

Many studies have shown that phase diversity (PD) is feasible and easy-implemented technology, and it can solve the problem of optical wavefront aberration or image restoration in the frequency domain [15–20]. Using the Zernike polynomials [21–23] to describe wave aberrations or lens optics, the PD can effectively and precisely obtain the PSF of the simple optical system and restore the blurred image. However, the PD is usually solved by a nonlinear optimization iterative algorithm that needs numerous matrix-vector computations, which is computationally complicated and time-consuming. Thus, it is difficult to directly use the PD for fast image restoration of the simple optical system.

To greatly shorten the restoration time while maintaining a good image quality, a fast image restoration method to eliminate the fixed optical aberration of the simple optical system utilizing the calibrated single-channel restoration factor is proposed in contrast to the dual-channel PD solved by nonlinear optimization iterative algorithms.

Specifically, the proposed method consists of three major steps. First, a method based on sine integral fitting is used to preprocess the image and the PSF of the simple optical system is estimated using the dual-channel PD in advance. Second, the single-channel restoration factor of the simple optical system is constructed in the frequency domain. Third, the blurred image can be directly and rapidly restored with the single-channel restoration factor.

The proposed method is required only twice Fourier transforms (FFTs) and can restore the blurred image of the simple optical system quickly. The effectiveness of this single-channel fast image restoration approach utilizing the constructed single-channel restoration factor is verified by experiment. The next section describes our methods used for the fast image restoration, followed by the simulation, experiment and finally the conclusion.

2. METHODS

The schematic of fast image restoration for the simple optical system is presented in Fig. 1 and consisted of two parts: calibration of single-channel restoration factor and fast image restoration.

The simple optical system can be approximately seen as a linear space-invariant system. Under incoherent illumination, the focal imaging model formula and the defocused imaging model formula can be written as Eqs. (1), (2) respectively

$$i(x,y)=o(x,y)*h(x,y)+n(x,y), \tag{1}$$

$$i_d(x,y)=o(x,y)*h_d(x,y)+n_d(x,y), \tag{2}$$

where, (x, y) is a two-dimensional coordinate in the image plane, i and i_d represent the actual focal target image and defocused target image received on image sensor respectively, the subscript represents d a known defocused distance of image sensor collection plane, o represents the ideal target image (assuming uniform illumination), * represents the convolution operation, n and n_d represent the noise of focal plane and defocused plane (for large enough photons, the noise can be approximated by an additive Gaussian noise, with zero mean and variance σ^2) respectively, h and h_d represent the focal PSF and the defocused PSF of the simple optical system respectively and are defined as [24] respectively

$$\begin{aligned} h(x,y)&=\left|\mathrm{F}^{-1}\{H\}\right|= \\ &=\left|\mathrm{F}^{-1}\left\{P(u,v)\exp\left[i\varphi(u,v)\right]\right\}\right|^2, \end{aligned} \tag{3}$$

$$\begin{aligned} h_d(x,y)&=\left|\mathrm{F}^{-1}\{H_d\}\right|= \\ &=\left|\mathrm{F}^{-1}\left\{P(u,v)\exp\left[i\varphi_d(u,v)\right]\right\}\right|^2, \end{aligned} \tag{4}$$

where, H and H_d are the generalized pupil functions, (u, v) is a two-dimensional plane coordinate in the pupil plane, F^{-1} represents the inverse Fourier transform, P is the pupil function, φ and φ_d are the wavefront phase of focal plane and defocused plane respectively, which can be decomposed into a set of Zernike polynomials

$$\varphi(u,v)=\sum_{q=1}^{M}a_q Z_q(u,v), \tag{5}$$

$$\varphi_d(u,v)=\theta_d(u,v)+\sum_{q=1}^{M}a_q Z_q(u,v), \tag{6}$$

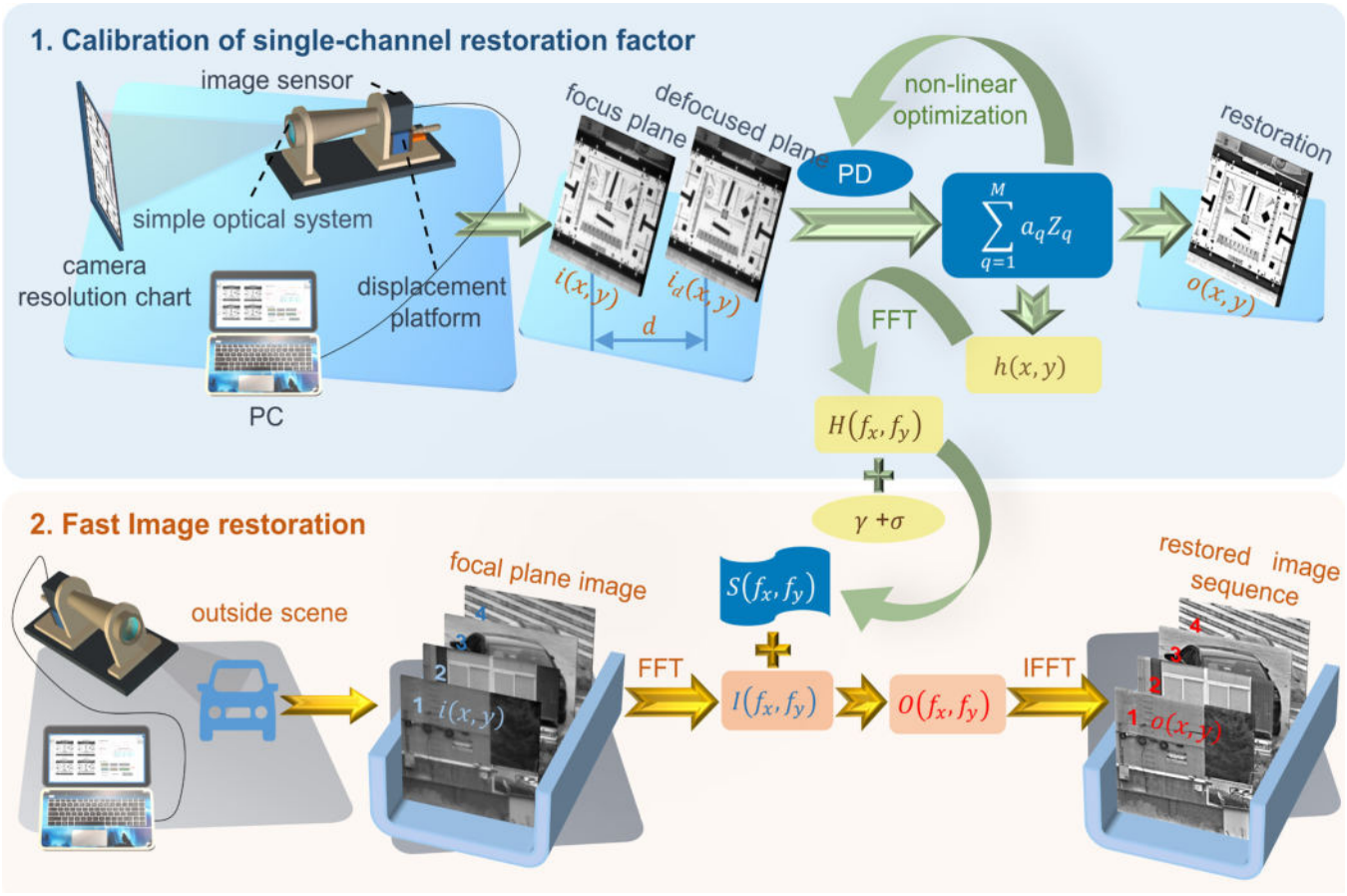


Fig. 1. Schematic of fast image restoration for the simple optical system.

$$\theta_d = \frac{2\pi}{\lambda}\Delta = \frac{2\pi}{\lambda}\frac{d}{8(f/D)^2}, \tag{7}$$

where, M is the maximum number of Zernike polynomials, a_q represents the Zernike coefficient, Z_q represents the basis Zernike polynomial, θ_d represents the known fixed-defocus phase, Δ represents the peak-to-valley (PV) defocus optical path distance, λ represents the wavelength, f represents the focal length of the optical system, and D represents the pupil diameter of the optical system. In the frequency domain, the focal and defocused imaging process can be expressed as Eqs. (8), (9) respectively

$$I(f_x,f_y) = O(f_x,f_y)H(f_x,f_y) + N(f_x,f_y), \tag{8}$$

$$I_d(f_x,f_y) = O(f_x,f_y)H_d(f_x,f_y) + N_d(f_x,f_y), \tag{9}$$

where, (f_x, f_y) is a two-dimensional complex plane coordinate, O, I, H, N, I_d, H_{di}, and N_d are the Fourier transform of o, i, h, n, i_d, h_d, and n_d respectively.

For the mathematical model of the PD dual-channel approach, the following error metric [25–28]

$$E(O,\{a_q\}) = \frac{1}{2N}\sum_{(f_x,f_y)}\left(\sigma^{-2}|I-OH|^2 + \sigma_d{}^{-2}|I_d - OH_d|^2 + \gamma|O|^2\right) \tag{10}$$

is usually used to evaluate the mean-squared image intensity difference between the data actually collected and the data predicted by optical system. N is the total number of pixels of a single image, σ and σ_d represent the additive Gaussian noise variance of focal plane and defocused plane, and γ is the regularization coefficient (to suppress noise and solve the problems with close to zero values in the blur kernel), which is non-negative.

Set $\partial E(O, \{a_q\})/\partial O$ to zero, we can obtain the solution of $O(f_x, f_y)$ –

$$O(f_x,f_y) = \frac{\sigma^{-2}I\bar{H} + \sigma_d{}^{-2}I_d\bar{H}_d}{\gamma + \sigma^{-2}|H|^2 + \sigma_d{}^{-2}|H_d|^2}, \tag{11}$$

where, $\bar{H}$ denotes the complex conjugate of H. Substituting Eq. (11) back to Eq. (10), we can obtain the error evaluation function

$$E\left(\left\{a_q\right\}\right)=\frac{1}{2N}\sum_{\left(f_x,f_y\right)}\left\{\sigma^{-2}|I|^2+{\sigma_d}^{-2}|I_d|^2-\right.$$
$$\left.-\frac{\left|\sigma^{-2}I\bar{H}+{\sigma_d}^{-2}I_d\bar{H}_d\right|^2}{\gamma+\sigma^{-2}|H|^2+{\sigma_d}^{-2}|H_d|^2}\right\}. \quad (12)$$

The error evaluation function in Eq. (12) is minimized with respect to a set of unknown Zernike coefficients by a nonlinear optimization routine. The partial derivative for $\{a_q\}$ according to Eqs. (3), (4), (11), and Eq. (12) can be expressed as

$$\begin{cases}\dfrac{\partial E}{\partial a_q}=\dfrac{-2}{N}\sum\limits_{(u,v)}Z_q(u,v)\mathrm{Im}\left(V\sigma^{-2}+V_d{\sigma_d}^{-2}\right)\\ V=\bar{H}\mathrm{F}\left\{h\,\mathrm{Re}\left[\mathrm{F}^{-1}\left(\bar{O}I-H|O|^2\right)\right]\right\}\\ V_d=\bar{H}_d\mathrm{F}\left\{h_d\,\mathrm{Re}\left[\mathrm{F}^{-1}\left(\bar{O}I_d-H_d|O|^2\right)\right]\right\}\end{cases}. \quad (13)$$

In these equations, the operators Re(•) and Im(•) take the real and imaginary part of the argument respectively. And then, the best Zernike coefficients can be utilized to calculate the PSF of the focal plane and restore the blur image. By combining the PSF of the focal plane, the additive Gaussian noise variance of the focal plane and the regularization coefficient, we can construct the single-channel restoration factor of the simple optical system as

$$S\left(f_x,f_y\right)=\frac{\sigma^{-2}\bar{H}}{\gamma+\sigma^{-2}|H|^2}. \quad (14)$$

The fast restored image by using the single-channel restoration factor of the simple optical system can be expressed as

$$o(x,y)=\mathrm{F}^{-1}\left\{O\left(f_x,f_y\right)\right\}=$$
$$=\mathrm{F}^{-1}\left\{I\left(f_x,f_y\right)S\left(f_x,f_y\right)\right\}. \quad (15)$$

3. SIMULATION

Assume the size of the Nyquist simulated sampled object was 1024×1024 pixels and the size of simulated pupil was 512×512 pixels. In dual-channel PD image restoration, the PV defocus optical path distance must be sufficiently large to ensure significant intensity differences between the focal surface image and the unfocal surface image to facilitate the nonlinear solution. For numerical simulation, the regularization coefficient γ and the PV defocus optical path distance Δ were set to be 1.0×10^{-5} and 1.0λ respectively. The simulation test did not account for the noise and the noise variance was set to be 1.0. We used the limited memory Broyden–Fletcher–Goldfarb–Shanno (L-BFGS) algorithm [29] to solve the Zernike coefficients of the error evaluation function due to its superior performance.

The root mean square error (RMSE) value of wavefront aberration is defined as follows:

$$\mathrm{RMSE}(\lambda)=$$
$$=\frac{1}{2\pi}\left\{\sum_{(u,v)}\left[\varphi_{\mathrm{rst}}(u,v)-\varphi_{\mathrm{ideal}}(u,v)\right]^2/N\right\}^{1/2}, \quad (16)$$

where, φ_{ideal} and φ_{rst} represent the ideal and restored wavefront aberration. Peak signal-to-noise ratio (PSNR) represents the level of image distortion, which can be presented as

$$\mathrm{PSNR}=$$
$$=10\log_{10}\left(\frac{o_{\max}^2}{\sum\limits_{(x,y)}\left[o_{\mathrm{rst}}(x,y)-o_{\mathrm{ideal}}(x,y)\right]^2/N}\right), \quad (17)$$

where, o_{ideal} and o_{rst} represent the ideal and restored image respectively, and $o_{\max}$ represents the maximum pixel value.

It can be seen in Fig. 2 that the RMSE between the ideal focus wavefront aberration and the restored focus wavefront aberration were 0.0558λ. The resolution, clarity and contrast of the restored images were obviously improved compared to the focal image. In addition, both the dual-channel and single-channel restored images (using the single-channel restoration factor to achieve fast image restoration with only twice FFTs) achieved PSNR values above 40.

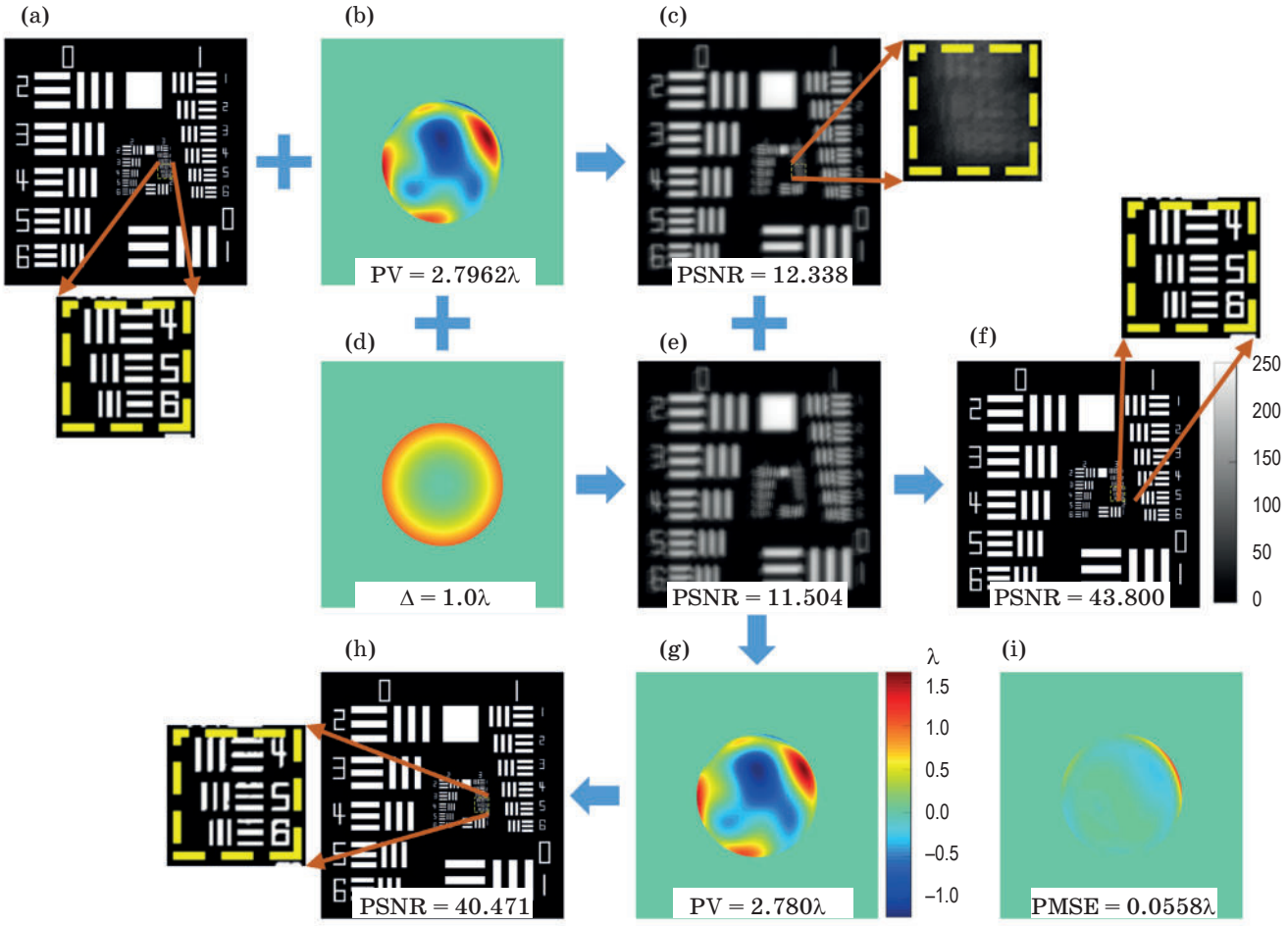


Fig. 2. Simulation results. (a), (c), (e), (f), and (h) were the ideal image, the focal image, the defocused image, the dual-channel restored image and the single-channel restored image respectively. (b), (d), and (g) were the ideal focus wavefront aberration, the additional defocus wavefront aberration and the restored focus wavefront aberration respectively. (i) was the wavefront residuals between (b) and (g).

Comparing Figs. 2h, f, it was clear that the single-channel restored image shown an identical image quality as with the dual-channel restored image. These results verified the validity of image restoration with PD. Meanwhile, the validity of single-channel image restoration was verified.

4. EXPERIMENT

4.1. Experiment setup

To further testify the validity of image restoration with dual-channel PD and single-channel fast image restoration, we performed a specific practical experiment. The basic model of the simple optical system was shown in Fig. 3a, which was equipped with the simple spherical lens and a manual displacement platform with precision of 0.01 mm. To detect the effect of image restoration with a telephoto optical system, we used the basic model to design two kinds of the simple optical system (the doublet spherical lens and triplet spherical lens) with the focal length of 175 mm and the aperture of 50.8 mm. Both the simple optical systems used randomized designs and belonged to the optical systems with small FOV. Thus, the two different optical systems mainly included severe on-axis aberrations (such as spherical aberration) and a small amount of off-axis aberrations (such as coma and astigmatism). Figure 3b was the calibration experiment of single-channel restoration factor and the fast image restoration experiment was presented in Fig. 3c. The other device parameters used for the experiment were shown in Table 1.

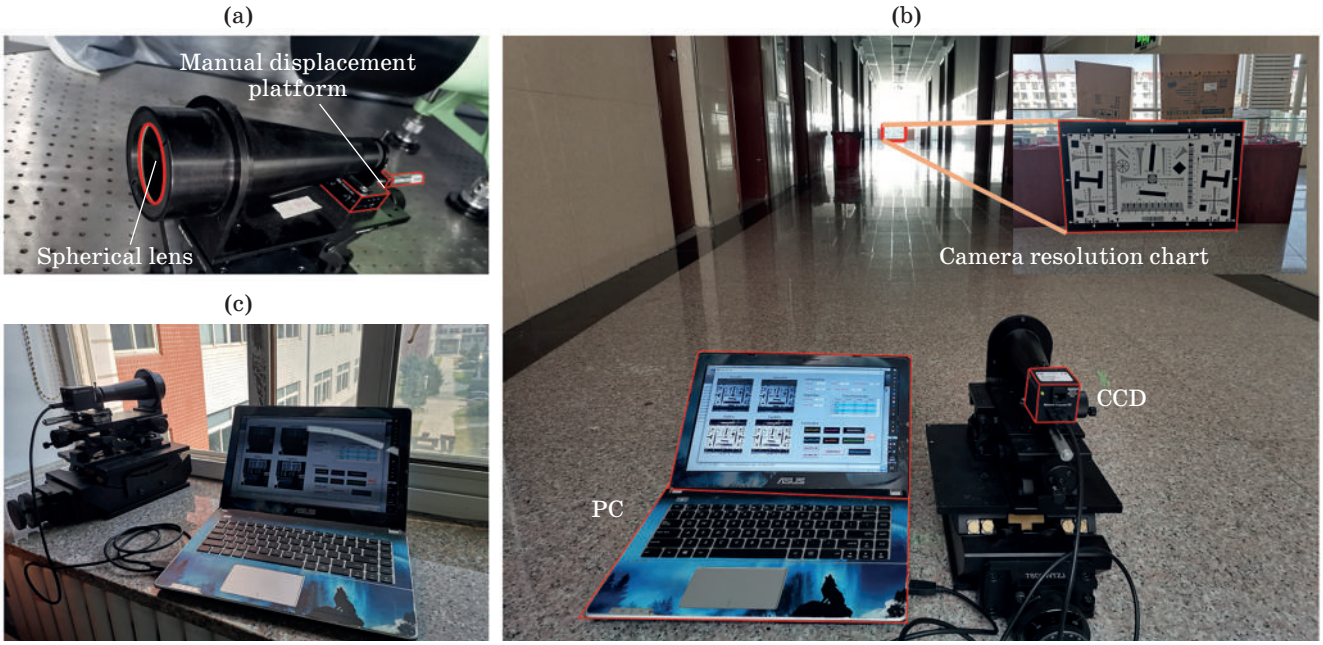


Fig. 3. Experimental setup. (a) The basic structure of the simple optical system, (b) the calibration experiment of single-channel restoration factor, (c) the fast image restoration experiment.

Table 1. Device parameters used for the experiment

Equipment name	Equipment parameter	Value
PC	CPU, GHz	Intel(R)Core(TM) i5-4200Hz @2.8
	RAM, GB	8.00
	Operating system	Win10 64-bit Operating System
	Calculating tool	Matlab2016a
CCD	Type	Lumenera Lm135M
	Max. resolution	1392×1040
	Pixel size, μm	4.65×4.65
	Output format	Mono 8-bit
Camera resolution chart	Size, mm	900×1550

4.2. Calibration of single-channel restoration factor

For the practical experiment, which does not have the ideal images, it is impossible to objectively evaluate the image quality with the full-reference image quality evaluation criteria and thus we applied some common non-reference image quality evaluation criteria, such as no-reference structural sharpness (NRSS) [30], information entropy (IE) [31, 32], and grayscale mean gradient (GMG) [33]. No-reference structural sharpness can characterize the image degradation degree caused by blurring or defocusing. Information entropy can be used to describe the richness of the image detail information and GMG represents the sharpness of the images. For all of these evaluation criteria, greater the value, greater is the image quality.

The specific process of calibration of single-channel restoration factor were described as follows:

(1) Determining the actual focus plane of the simple optical system

First, we used the camera resolution chart as the target of CCD with the relative distance of approximately 40 m, and then the manual dis-

placement platform was fine-tuned to adjust the position of CCD with respect to the ideal focus plane of the simple optical system. Combining with NRSS, IE and GMG to evaluate the image quality, we determined the actual focus plane of the simple optical system.

(2) Recording the focus and defocused image

We recorded some focus images of the camera resolution chart on the actual focus plane of the simple optical system with CCD. Then, adjusting CCD to the defocused plane via fine-tuning of the manual displacement platform, we recorded some defocused images of the camera resolution chart. The empirical value of the PV defocus optical path distance Δ is 1.0λ. Since we chose the optimal response wavelength (510 nm) of CCD sensor as the center wavelength λ, the corresponding values for defocused distance d was approximately 0.05 mm according to Eq. (7). Stability of the manual displacement platform required attention during the image acquisition process.

(3) Calibrating the single-channel restoration factor

To speed up the operation speed and maximize the use of image information, the images were cropped (1024×1024 pixels) from the original images (1392×1040 pixels). The regularization coefficient γ was empirically set to be 1.0×10^{-4}. The focal image and the defocused image had the same noise level because they were from the same CCD, so the noise variance σ and σ_d were both set to 1. Following the methods of Sec. 2, we can get the single-channel restoration factor.

In the practical experiment, blind image restoration based on the frequency domain usually results in serious border ringing effect owing to boundary discontinuity. To remedy this issue, we used a method with sine integral fitting to preprocess the image [34]. The preprocessing steps were given in Fig. 4.

Figures 5 and 6 compared the image restoration results obtained by the dual-channel PD and the single-channel fast image restoration. Simultaneously, the image restoration results were compared with and without image preprocessing. It can be seen in Figs. 5 and 6 that the improvement in all restored images quality was clear, both qualitatively and quantitatively. The resolution, clarity and contrast of the restored images were obviously improved compared to

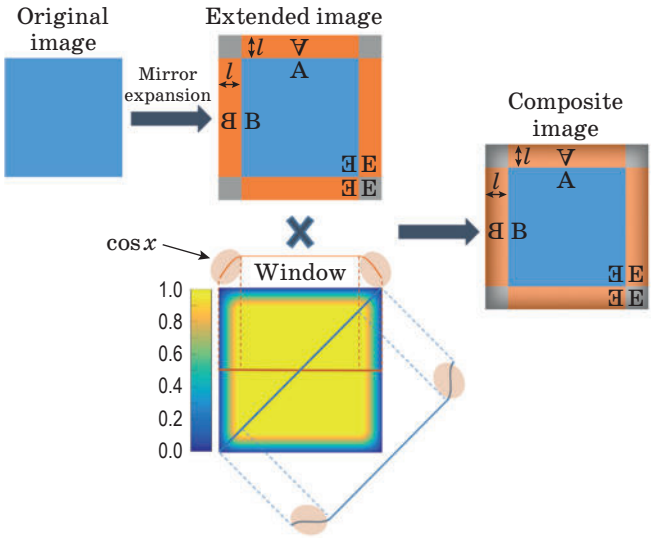


Fig. 4. Image preprocessing with sine integral fitting. First, we extended the original image based on mirror expansion. The extended length l was determined based on the size of blur kernel (PSF). Then, the window function was synthesized using the method of sine integral fitting based on the size of extended image. Finally, the composite image can be obtained by combined the extended image with window function.

the focal images. However, the border ringing effect of restored image was greatly suppressed with image preprocessing. For instance, as seen from the enlarged details A and B of Figs. 6b, c, compared to the restored image without image preprocessing, the border of the restored image with image preprocessing was more distinct. Both the dual-channel and single-channel restored images of the two different optical systems can get higher quality with image preprocessing. At the same time, the single-channel restored image showed an identical image quality as with the dual-channel restored image with image preprocessing. This further illustrated the validity of single-channel fast image restoration.

4.3. Fast image restoration experiment

We further performed a fast image restoration experiment for the validity of single-channel fast image restoration. First, some focus images of different targets (the distance of CCD to the imaged target was greater than 300 m) were acquired by the doublet and triplet lens system during the day. Then the focus images were restored with the calibrated single-channel restoration factor respectively.

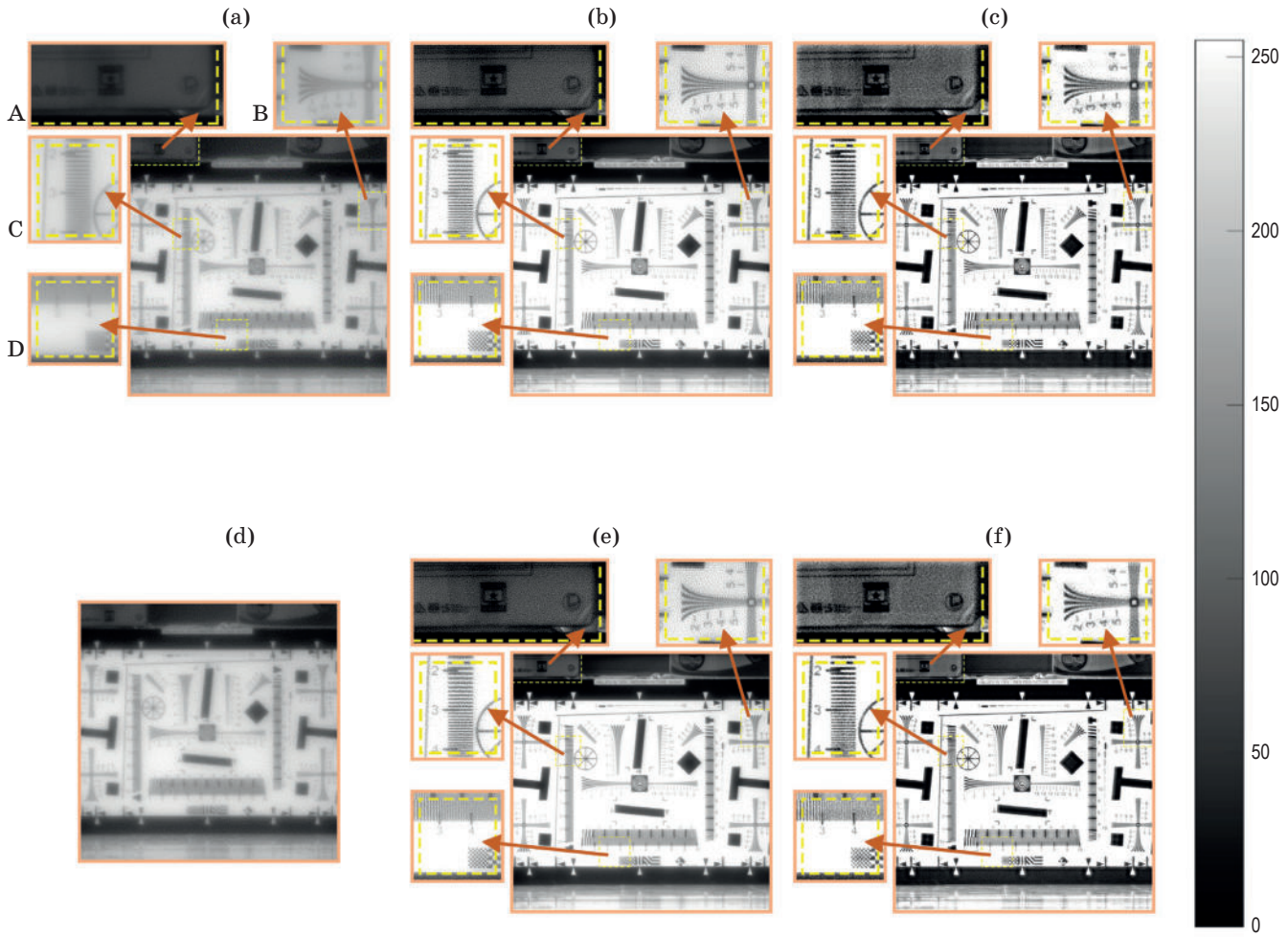


Fig. 5. Calibration results of the doublet lens system. (a, GMG = 0.0036, IE = 6.6058, NRSS = 0.1470) and (d) were the focal and defocused image respectively. (b, GMG = 0.0136, IE = 7.2603, NRSS = 0.2029) and (e, GMG = 0.0133, IE = 7.2112, NRSS = 0.2035) were the dual-channel and single-channel restored image without image preprocessing respectively. (c, GMG = 0.0173, IE = 7.3103, NRSS = 0.2129) and (f, GMG = 0.0173, IE = 7.2908, NRSS = 0.2104) were the dual-channel and single-channel restored image with image preprocessing respectively.

It can be seen visually in Figs. 7 and 8 that the improvement in all restored images quality was clear. However, as expected, compared with the restored image without image preprocessing, the restored images with image preprocessing had larger information content and higher distinguishability of details. Meanwhile, the contrast of the restored images with image preprocessing was further enhanced and the edges of the image were more distinct compared to the restored image without image preprocessing. In particular, the restored image quality of the doublet lens system was close to or even more than the focus image quality of the triplet lens system. The qualitative evaluation was confirmed by the quantitative results reported in Table 2, which showed the image restoration performance obtained by the single-channel fast image restoration with image preprocessing in terms of GMG, NRSS and IE. These indexed demonstrate the validity of the single-channel fast image restoration.

4.4. Discussion

The dual-channel image restoration is solved by a nonlinear optimization iterative algorithm that needs a large number of FFTs, which is computationally complicated and time-consuming. However, the single-channel fast image restoration required only twice FFTs without iterative op-

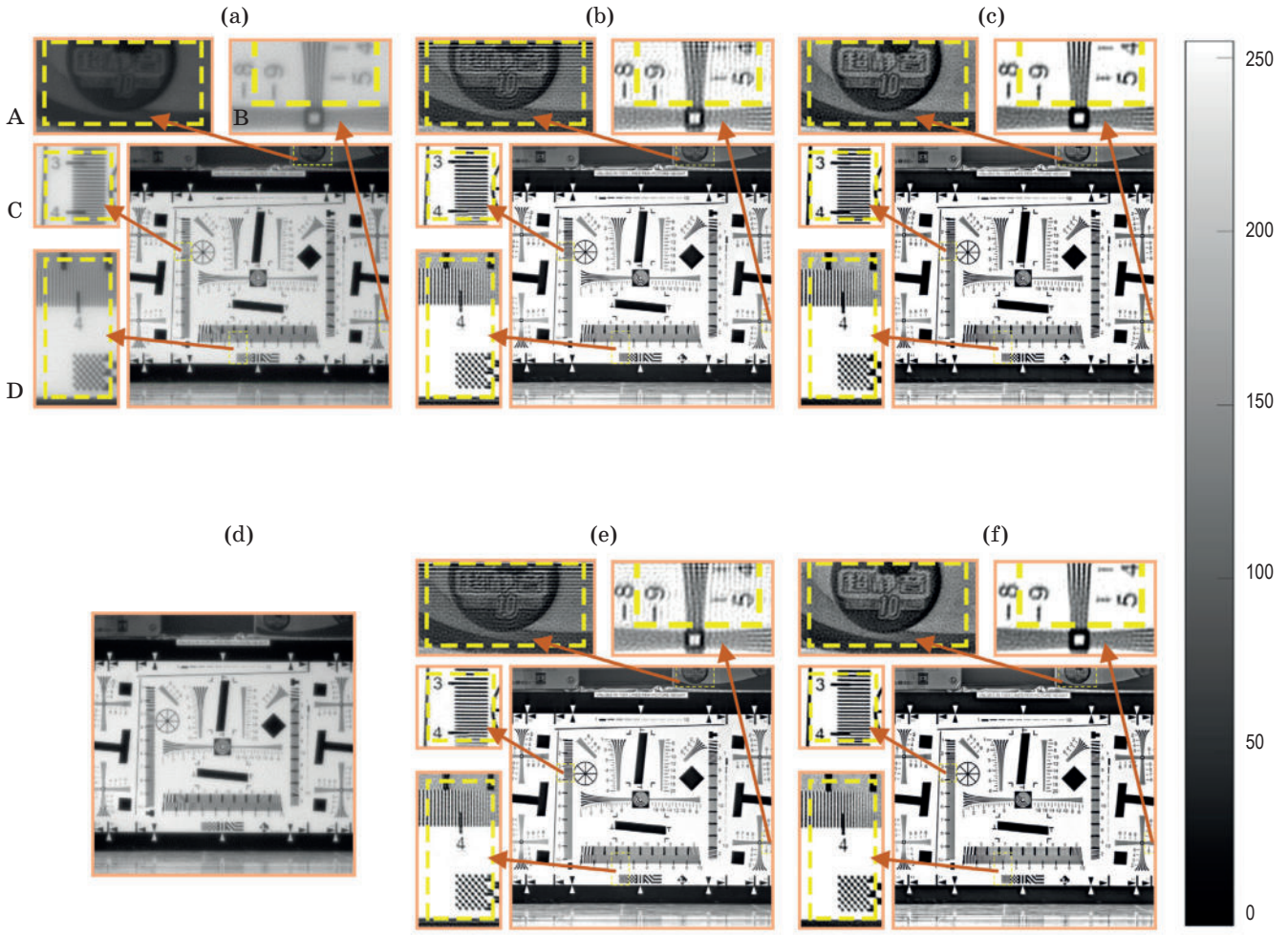


Fig. 6. Calibration results of the triplet lens system. (a, GMG = 0.0066, IE = 6.8710, NRSS = 0.1381) and (d) were the focal and defocused image respectively. (b, GMG = 0.0250, IE =7.7553, NRSS = 0.1921) and (e, GMG = 0.0249, IE = 7.8706, NRSS = 0.1920) were the dual-channel and single-channel restored image without image preprocessing respectively. (c, GMG = 0.0264, IE = 8.0956, NRSS = 0.1959) and (f, GMG = 0.0264, IE = 8.0509, NRSS = 0.1958) were the dual-channel and single-channel restored image with image preprocessing respectively.

timization can directly and rapidly restore the blurred image using the calibrated single-channel restoration factor. The comparison result of the image restoration time had been presented in Table 3, which demonstrated the advantage of single-channel fast image restoration. We can see that the average restoration time was reduced by the factors of 3962.31 and 2133.24 on two different simple optical systems with the single-channel image restoration relative to the dual-channel image restoration respectively. Note that the average restoration time of the dual-channel image restoration is determined by both the aberrations and the distance between the initial value and the optimal value. Thus, the restoration time is also varied for the same initial value to the different optical systems based on the dual-channel image restoration. Overall, the method for image restoration based on the calibrated single-channel restoration factor, which is required only twice FFTs without iterative optimization, can get an identical image quality as with the dual-channel image restoration while dramatically decreasing the image restoration time. But one thing still needs to be pointed out, the proposed method and experiment are designed to remove the fixed optical aberration of a telephoto optical system (long focal length and small FOV), and the PSF is approximately spatially invariant. If the proposed

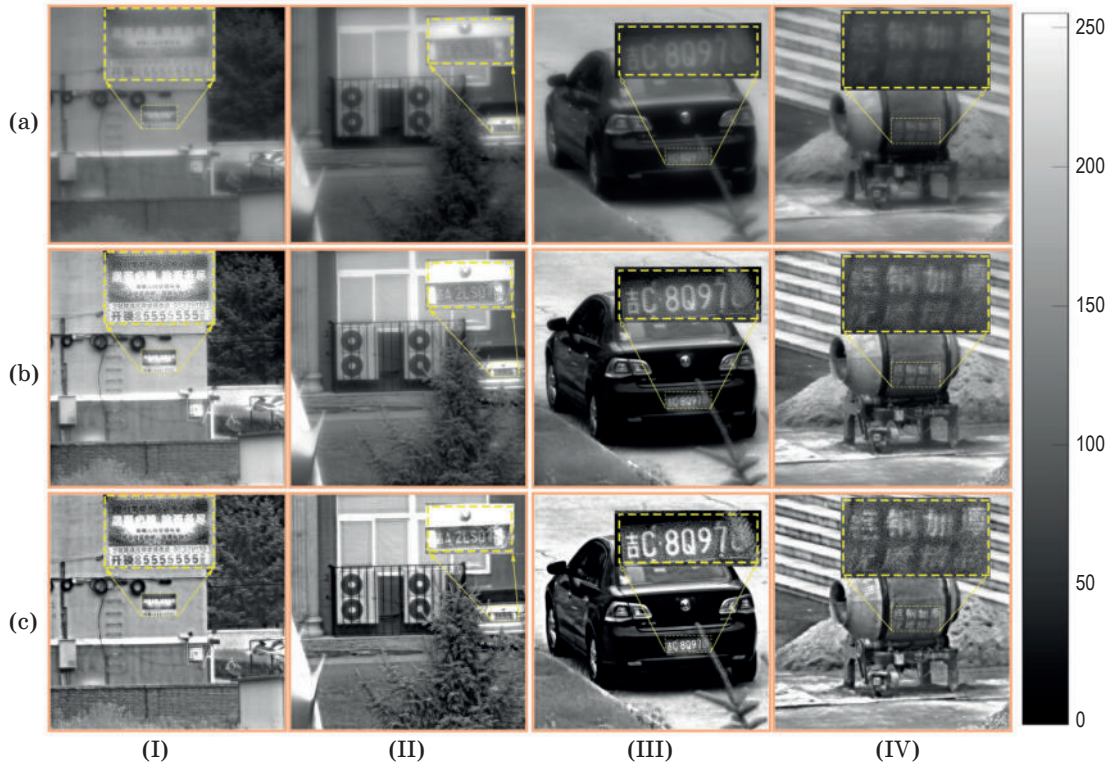


Fig. 7. Fast image restoration results of the doublet lens system. (a) The focus image, (b) the restored image without image preprocessing, (c) the restored image with image preprocessing. The yellow dashed box indicated the partial details and their enlarged region.

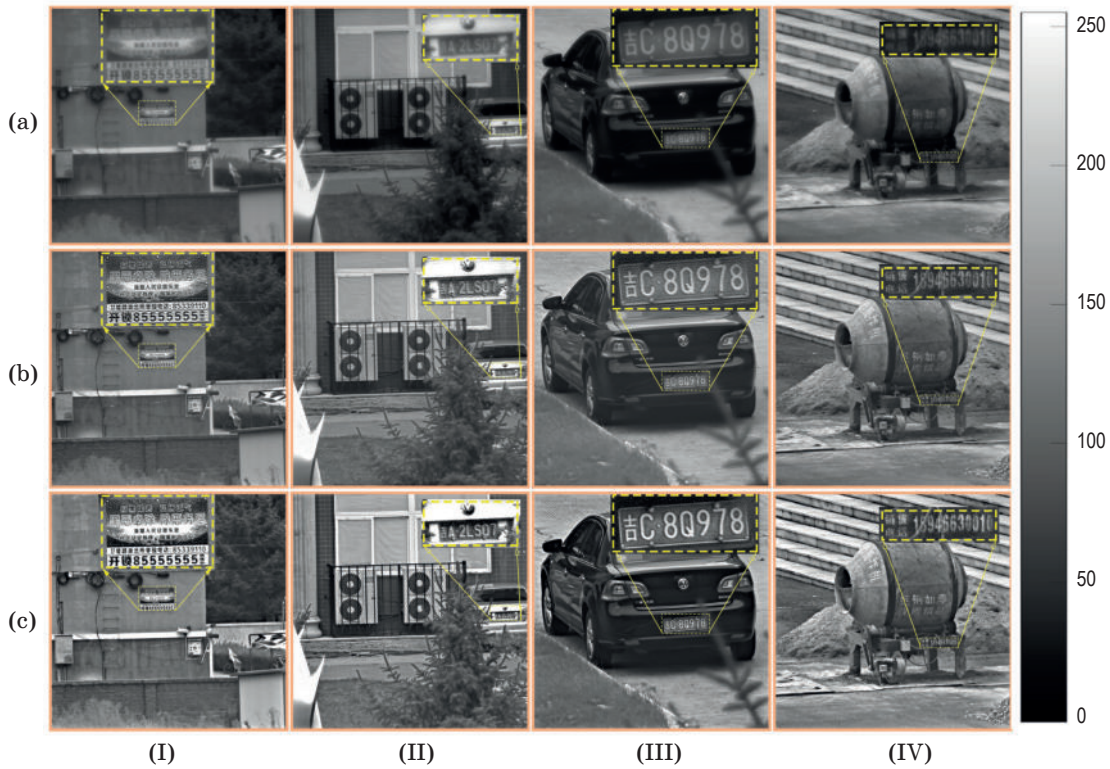


Fig. 8. Fast image restoration results of the triplet lens system. (a) The focus image, (b) the restored image without image preprocessing, (c) the restored image with image preprocessing. The yellow dashed box indicated the partial details and their enlarged region.

Table 2. Image quality evaluation of fast image restoration

Optical system	Evaluation method	Figs. 7 and 8	(I)	(II)	(III)	(IV)
Doublet lens	GMG	(a)	0.00386	0.00344	0.00324	0.00412
		(b)	0.01614	0.01047	0.01161	0.01202
		(c)	**0.01649**	**0.01409**	**0.01417**	**0.01351**
	NRSS	(a)	0.08073	0.09379	0.06616	0.07483
		(b)	0.11593	0.11924	0.11567	0.10148
		(c)	**0.12554**	**0.12074**	**0.15837**	**0.12911**
	IE	(a)	5.88470	6.43908	6.41590	6.21392
		(b)	7.76299	7.64730	7.33676	7.68348
		(c)	**7.86224**	**7.72571**	**7.50779**	**7.81788**
Triplet lens	GMG	(a)	0.00393	0.00429	0.00367	0.00462
		(b)	0.01263	0.01236	0.01084	0.01267
		(c)	**0.01504**	**0.01376**	**0.01181**	**0.01469**
	NRSS	(a)	0.07335	0.09285	0.09550	0.11611
		(b)	0.10126	0.10384	0.11278	0.15503
		(c)	**0.11607**	**0.11824**	**0.12564**	**0.16465**
	IE	(a)	5.80005	6.44032	6.52334	6.50621
		(b)	7.18711	7.47063	7.45247	7.55637
		(c)	**7.39271**	**7.55861**	**7.65711**	**7.71546**

Note. (a) The focus image, (b) the restored image without image preprocessing, (c) the restored image with image preprocessing (see Figs. 7, 8)

Table 3. Image restoration time with image preprocessing

Optical system	Method	Average restoration time, ms	Number of iterations
Doublet lens	dual-channel	328872	86
	single-channel	**83**	0
Triplet lens	dual-channel	174926	34
	single-channel	**82**	0

method is to be applied to an optical system with large FOV, it will be necessary to use a set of spatially varying point spread functions [35] to respond to large amounts of severe off-axis aberrations.

5. CONCLUSION

In summary, we propose a fast image restoration method using the dual-channel PD and the calibrated single-channel restoration factor to remove the fixed optical aberration of the simple optical system. The method based on sine integral fitting is used to preprocess the image. And then the Zernike polynomials are used to build the wavefront aberration model of the simple optical system. We use the L-BFGS algorithm to solve the Zernike coefficients of the dual-channel PD and then calculate PSF of the simple optical system. Finally, we use the PSF to construct the single-channel restoration factor for directly and rapidly restoring the blurred image of the simple optical system. Our experimental results with two different simple optical systems verify

the fast image restoration ability of the method based on the single-channel restoration factor. Compared to the dual-channel image restoration, this single-channel fast image restoration approach is lower in computational load and higher in efficiency (only need twice FFTs without iterative optimization), and can quickly restore the blurred image. Our on-going effort is to simplify the design process and structure of the telephoto optical system for clear observation in the UAV and astronomical exploration, and our results may result in further cost savings.

This work was supported by Ministry of Science and Technology Project (2018YFB1107600) and Jilin Scientific and Technological Development Program (20160204009GX, 20170623004TC, 20170204014GX).

REFERENCES

1. *Zheng G., Horstmeyer R., Yang C.* Wide-field, high-resolution Fourier ptychographic microscopy // Nat. Photonics. 2013. V. 7. № 9. P. 739–745.
2. *Sun J.S., Qian C., Zhang Y.Z., Zhao Z.* Efficient positional misalignment correction method for Fourier ptychographic microscopy // Biomed. Opt. Exp. 2016. V. 7. №. 4. P. 1336–1350.
3. *Faulkner H.M.L., Rodenburg J.M.* Movable aperture lensless transmission microscopy: A novel phase retrieval algorithm // Phys. Rev. Lett. 2004. V. 93. № 2. P. 023903.
4. *Shen C., Bao X.J., Tan J.B., Liu S.T.* Two noise-robust axial scanning multi-image phase retrieval algorithms based on Pauta criterion and smoothness constraint // Opt. Exp. 2017. V. 25. № 14. P. 16235.
5. *Shao X., Dai X., He X.* Noise robustness and parallel computation of the inverse compositional Gauss–Newton algorithm in digital image correlation // Opt. Lasers Eng. 2015. V. 71. P. 9–19.
6. *Schuler C.J., Hirsch M., Harmeling S., Scholkopf B.* Non-stationary correction of optical aberrations // ICCV. Barcelona, Spain. 2011. P. 659–666.
7. *Heide F., Rouf M., Hullin M.B., Labitzke B.* High-quality computational imaging through simple lenses // ACM Trans. Graph. 2013. V. 32. № 5. P. 1–14.
8. *Li W.L., Yin X.Q., Liu Y., Zhang M.J.* Computational imaging through chromatic aberration corrected simple lenses // J. Mod. Opt. 2017. V. 64. № 20. P. 2211–2220.
9. *Cui J., Huang W.* Optical aberration correction for simple lenses via sparse representation // Opt. Commun. 2018. V. 412. P. 201–213.
10. *Peng Y.F., Fu Q., Amata H.* Computational imaging using lightweight diffractive-refractive optics // Opt. Exp. 2015. V. 23. № 24. P. 31393.
11. *Heide F., Fu Q., Peng Y.F.* Encoded diffractive optics for full-spectrum computational imaging // Sci. Rep. 2016. V. 6. № 1.
12. *Nikonorov A., Evdokimova V.V., Petrov M.* Deep learning-based imaging using single-lens and multi-aperture diffractive optical systems // ICCVW. Seul, Korea. 2019. P. 3969–3977.
13. *Peng Y.F., Sun Q.L., Dun X.* Learned large field-of-view imaging with thin-plate optics // ACM Trans. Graph. 2019. V. 38. № 6. P. 1–14.
14. *Schmidt J.D., Jackovitz K., Riley J.T.* Real-time image restoration for space-object imaging // Appl. Opt. 2019. V. 58. № 25. P. 6983.
15. *Zhang P.G., Yang C.L., Xu Z. H.* Hybrid particle swarm global optimization algorithm for phase diversity phase retrieval // Opt. Exp. 2016. V. 24. № 22. P. 25704.
16. *Dolne J.J., Menicucci P., Miccolis D.* Advanced image processing and wavefront sensing with real-time phase diversity // Appl. Opt. 2009. V. 48. № 1. P. A30.
17. *Védrenne N., Mugnier L.M., Michau V.* Laser beam complex amplitude measurement by phase diversity // Opt. Exp. 2014. V. 22. № 4. P. 4575
18. *Zhang D., Zhang X.B., Xu S.Y.* Simplified phase diversity algorithm based on a first-order Taylor expansion // Appl. Opt. 2017. V. 55. № 28. P. 7872.
19. *Cheng Q., Zhang Y.D., Gao W.* Restoration of broadband light illumination image using phase diversity technology // AOMATT. Harbin, China. 2014. V. 9282. P. 928206.
20. *Zhang S., Wang B., Zhao J.* High resolution optical image restoration for ground-based large telescope using phase diversity speckle // Optik. 2014. V. 125. № 2. P. 861–864.
21. *von Zernike F.* Beugungstheorie des schneidenver-fahrens und seiner verbesserten form, der phasenkontrastmethode // Physica. 1934. Bd. 1. № 7. S. 689–704.

22. *Noll R.J.* Zernike polynomials and atmospheric turbulence // JOSA. 1976. V. 66. № 3. P. 207–211.
23. *Janout P., Páta P., Skala P.* PSF estimation of space-variant ultra-wide field of view imaging systems // Appl. Sci. 2017. V. 7. № 2. P. 151.
24. *Roggemann M.C.* Imaging through turbulence // Opt. Eng. 1996. V. 35. № 11. P. 3361.
25. *Gonsalves R.A.* Phase retrieval and diversity in adaptive optics // Opt. Eng. 1982. V. 21. № 5. P. 19–22.
26. *Paxman R.G., Schulz T.J., Fienup J.R.* Joint estimation of object and aberrations by using phase diversity // JOSA. A. 1992. V. 9. № 7. P. 1072–1085.
27. *Ma X.X., Wang J.L., Wang B.* Phase diversity for calibrating noncommon path aberrations of adaptive optics system under nonideal measurement environment // Optik. 2014. V. 125. № 17. P. 5029–5035.
28. *Gilles L., Vogel C.R., Bardsley J.M.* Computational methods for a large-scale inverse problem arising in atmospheric optics // Inverse Probl. 2006. V. 18. № 1. P. 237–252.
29. *Liu D.C., Nocedal J.* On the limited memory BFGS method for large scale optimization // Math. Program. 1989. V. 45. № 1–3. P. 503–528.
30. *Xie X.F., Zhou J., Wu Q.Z.* Assess image blur in photoelectric imaging system // 5th Int. Symp. Adv. Opt. Manuf. Test. Technol. Dalian, China. 2010. V. 7658. P. 765803–765806.
31. *Shannon C.E.* A mathematical theory of communication // Bell Syst. Tech. J. 1948. V. 27. № 3. P. 379–423.
32. *Barnum H., Barrett J., Clark L.O.* Entropy and information causality in general probabilistic theories // New J. Phys. 2010. V. 12. № 3. P. 033024.
33. *Huang W., Jing Z.* Evaluation of focus measures in multi-focus image fusion // Pattern Recognit. Lett. 2007. V. 28. № 4. P. 493–500.
34. *Zhao M.H., Zhang X., Shi Z.H.* Border ringing effects suppression of a restored image with sine integral fitting // J. Image Graph. V. 22. № 2. P. 0249–0256.
35. *Song P., Jiang S.W., Zhang H.* Full-field Fourier ptychography (FFP): Spatially varying pupil modeling and its application for rapid field-dependent aberration metrology // APL Photonics. 2019. V. 4. № 5. P. 050802.